Supporting Information

Hollow polydopamine spheres decorated with MoS_2 nanosheets for hydrogen evolution reaction

Raphaella T. S. Gonçalves[a,b], Matheus F. F. das Neves[c], Carlos Ospina[c] and Murilo Santhiago[a,c]**

[a] Federal University of ABC, Santo André, São Paulo 09210-580, Brazil

[b] Ilum School of Science Brazilian Center for Research in Energy and Materials, Campinas, São Paulo 13083-970, Brazil

[c] Brazilian Nanotechnology National Laboratory, Brazilian Center for Research in Energy and Materials, Campinas, São Paulo 13083-970, Campinas, Brazil

*e-mail: murilo.santhiago@lnnano.cnpem.br

Experimental section and methods

Chemical. Ethyl Alcohol Absolute [C_2H_6O, 99,5%, Synth], tetraethyl orthosilicate [TEOS, $Si(OC_2H_5)_4$, 99,5%, Sigma Aldrich, 759414] and ammonium hydroxide [NH_4OH, 30%, Synth, H1010] were used for the synthesis of colloidal silica sub-microparticles. Dopamine hydrochloride [DAH, 98%, Sigma Aldrich, H8502] and Tris(hydroxymethyl)-aminomethane buffer [$C_4H_{11}NO_3$, 99,9%, Promega, H5135] were used for polydopamine shell polymerization. Sodium molybdate [Na_2MoO_4, 98%, Sigma Aldrich, 243655] and L-cysteine [$HSCH_2CH(NH_2)COOH \cdot HCl \cdot H_2O$, 99%, Sigma Aldrich, 30129] were used as precursors of the MoS_2 nanosheets. NaOH 1M were used for silica core removal. Hydrophilic Millipore PTFE Filtration Membrane 1.0 μm to separate SiO_2@PDA from unattached polymers and 0.22 μm to separate HCS from high alkaline medium after silica removal and MoS_2@HCS from reaction medium. Sulphuric acid [H_2SO_4, 95%, Sigma Aldrich, A1060] 0.5 M, as an electrolyte to evaluate the stability and electrocatalytic activity in acidic media. All the chemicals used in this study were purchased and used without further purification.

Synthesis of HCS. The synthesis of the sub-microparticles of SiO_2 were performed by the sol-gel method, using TEOS as a precursor of silicon. The reaction was conducted in pH 10.5 using ammonium hydroxide as a catalyst for the reaction. In a volumetric flask, TEOS (2 mL) was added to ethanol (50 mL) and the solution was subjected to magnetic stirring for 30 min. Subsequently, NH_4OH (10 mL) was added to the mixture and the reaction continued in magnetic stirring for 3 hours. Soon after, the same amount of TEOS was added to the reaction and the system was kept in magnetic agitation for 24 hours at room temperature. Silica washing occurred by centrifugation at 10000 rpm for 15 min to remove the reaction medium. Then, the sub-microparticles were washed in ethanol (1x) and water (4x). The coating of SiO_2 sub-microparticles was performed by dispersing the silica in tris buffer (10 mM, pH 8.5) containing DAH (2.0 mg mL^{-1}). The reaction was maintained in magnetic stirring at room temperature for a certain time (24 – 48h) to control the thickness of PDA. Washing occurred with the removal of the reaction medium using a centrifuge at 10000 rpm for 15 min. The SiO_2@PDA were washed in water (2x) and ethanol (2x) and filtered by means of a filter (1.0 μm) with a pumping system.

HCS preparation was performed after drying the SiO_2@PDA in an oven at 60 °C for 24 hours. Then, the SiO_2@PDA were subjected to a heat treatment process to improve the mechanical stability. The heating process was conducted using a tube furnace under an atmosphere of N_2 at 400 °C for 2 hours with a heating rate at 5 °C/min to avoid rapid mass loss. This process is important to prevent PDA from dissolving along with silica in chemical treatment, as well as providing a rigid structure for hydrothermal synthesis. In the selective chemical attack for removal of the silica core from the core-shell compound, the black powder obtained was dispersed in NaOH 1.0 M and maintained in magnetic agitation. The sub-microparticles were filtered in a filter system with pumping, using a 0.22 μm PTFE membrane. The retained material was redispersed in ethanol.

Synthesis of HCS@MoS_2. The synthesis of the HCS@MoS_2 were performed by using a hydrothermal process. The experiment consisted of adding 50 mg of sodium molybdate and 100 mg of L-cysteine in 25

mL of ultrapure water under magnetic stirring for 1 hour for the complete dissolution of the precursors. Simultaneously, HCS were dispersed in ultrapure water and ultrasonicated for 30 min. Then, HCS were added to the solution and stirred until complete dispersion in the solution. The synthesis was poured into a Teflon capsule, inserted into the autoclave reactor, sealed and kept in a muffle furnace at 200 °C for 20 hours. The reaction products were washed by centrifugation at 10000 rpm for 15 min in water (3x) and ethanol (3x). To evaluate the electrocatalytic activity, the HCS@MoS_2 were deposited on pyrolyzed paper (PP) electrodes obtained according to the literature[1]. Briefly, Whatman #1 filter paper strips were pyrolyzed in a tubular furnace at 1000 °C for 1 hour to obtain highly conductive electrodes. Cooling occurred naturally at room temperature.

Preparation of the electrode and electrochemical measurements. The electrochemical assays were based on a three-electrode system using glassy carbon electrode as counter electrode (CE), Ag/AgCl as reference electrode (RE) and modified pyrolyzed paper as working electrode (WE). The working electrode and silver contact pads were prepared as reported [2]. 100 µL of a dispersion of HCS@MoS_2 2mg mL^{-1} in water were dropped on PP. The geometric area of the working electrode was 3.14×10^{-2} cm^2. Before the electrochemical measurements the electrolyte was purged with N_2 for 1h. The electrochemical tests were carried out in the Autolab potentiostat, model PGSTAT204, from Metrohm. The electrochemically active area was calculated by obtaining cyclic voltammograms in a non-faradaic region at different scan rates (5 – 100 mV s^{-1}). HER analysis was performed at a scan rate of 5 mV s^{-1}. The software NOVA version 2.1.6 software was used for data acquisition. Pristine MoS_2 flakes (3.33 mg mL^{-1}) from Sigma-aldrich were deposited on PP electrodes as comparison[2].

Experimental techniques. The particle size was measured in aqueous medium using dynamic light scattering (DLS) using a Malvern Zetasizer Ultra instrument. The chemical characterization of MoS_2 was obtained by XPS using a Thermo K-Alpha Surface Analysis instrument. The XPS data were processed using Avantage software version V5.9931. The morphology, coating of MoS_2 nanosheets and hollow structure of the particles were analyzed by scanning electron microscopy (SEM), using the FEI Quanta 650 FEG microscope, voltage of 5kV and 20kV, spot size of 3.0, objective lens aperture of 30 mm, working distance (WD) of 6 mm and Everhart Tornley Detector (ETD) in secondary electron (SE) mode. The images were processed using the ImageJ software version 2.1.0. The thickness of the hollow carbon sphere, the crystal structure and the electron diffraction were obtained by transmission electron microscopy (TEM), using the JEM-2100F microscope (JEOL), accelerating voltage 200 kV, operating in parallel and probe modes. The EDS detector used was the X-MaxN 80 TLE (Oxford Instruments) with the acquisition and processing software AZtec (version 3.3). The samples were dispersed and deposited on a 3 mm circular copper grid with ultrathin carbon film on lacey carbon support film, 400 mesh, with prior treatment in the easiGlow equipment. Thermal gravimetric analysis of PDA was performed using STA 449 F3 Jupiter thermal instrument from NETZSCH. The analyses were performed with approximately 10 mg of each powder sample inserted into an alumina oxide Al_2O_3 crucible. The heating range was between 25 °C and 1000 °C, at a gradual heating rate maintained at 5 °C/min under synthetic air flow.

Silica sub-microparticles

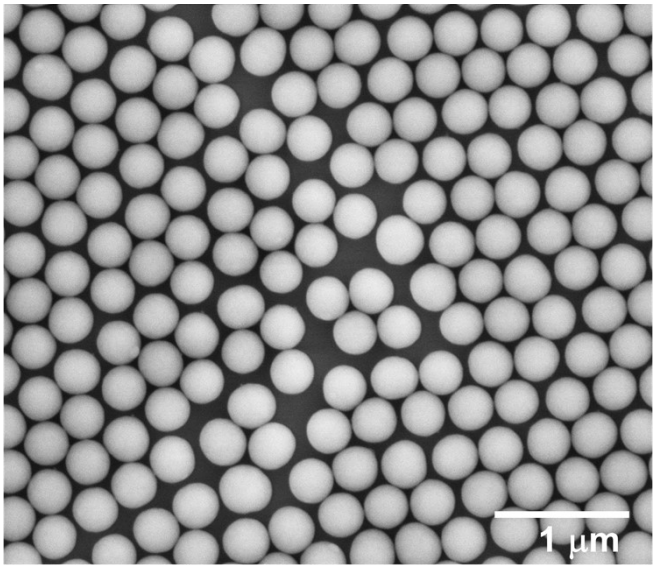

Figure S1. SEM image of the SiO_2 sub-microparticles.

Dynamic light scattering and comparison with MEV size distribution

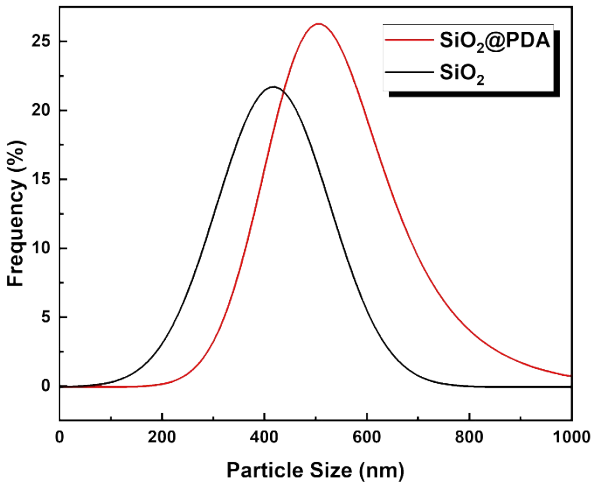

Figure S2. DLS measurement of SiO_2 and SiO_2@PDA indicating PDA coating with ~100 nm.

Thermogravimetric analysis of HCS and MoS_2 decomposition

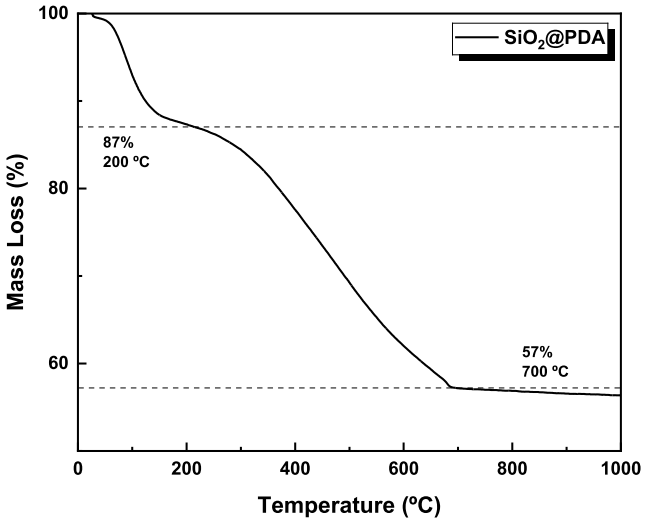

Figure S3. TGA of the SiO_2@PDA sample.

Raman Spectra

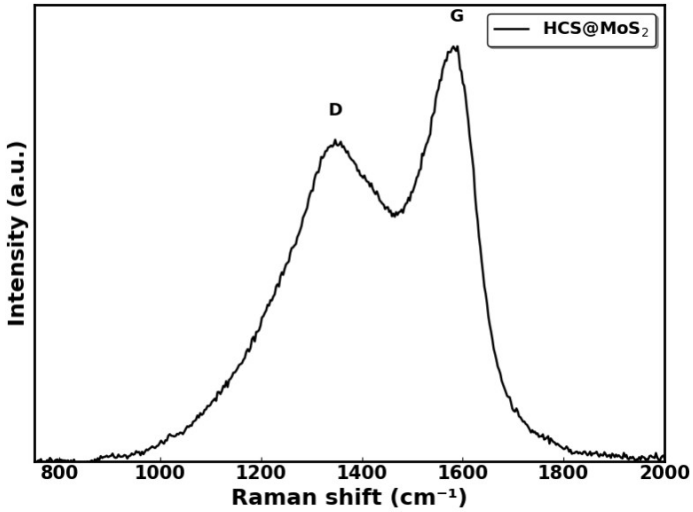

Figure S4. Raman of HCS@MoS_2 acquired with 532 nm laser, indicating the D e G characteristic graphitic carbon bands.

Crystalline Fringes of MoS_2 analysis

Figure S5(a) shows the high-resolution TEM image of the HCS@MoS_2 nanosheets selected for crystallinity assessment. In this image, lattice fringes corresponding to the interlayer separation of MoS_2 (~0.6 nm) can also be observed, and the regions selected for analysis are highlighted. The corresponding Fast Fourier Transform (FFT), obtained from the marked area, is presented in Figure S5(b). The FFT pattern displays discrete reciprocal-space spots with measured d-spacings in the 0.250–0.262 nm range, indicating well-defined lattice periodicity[3,4]. These values are consistent with the expected in-plane structural ordering of crystalline MoS_2 and complement the lattice fringes visible both in Figure S5(a) and in Figure 2h of the main text.

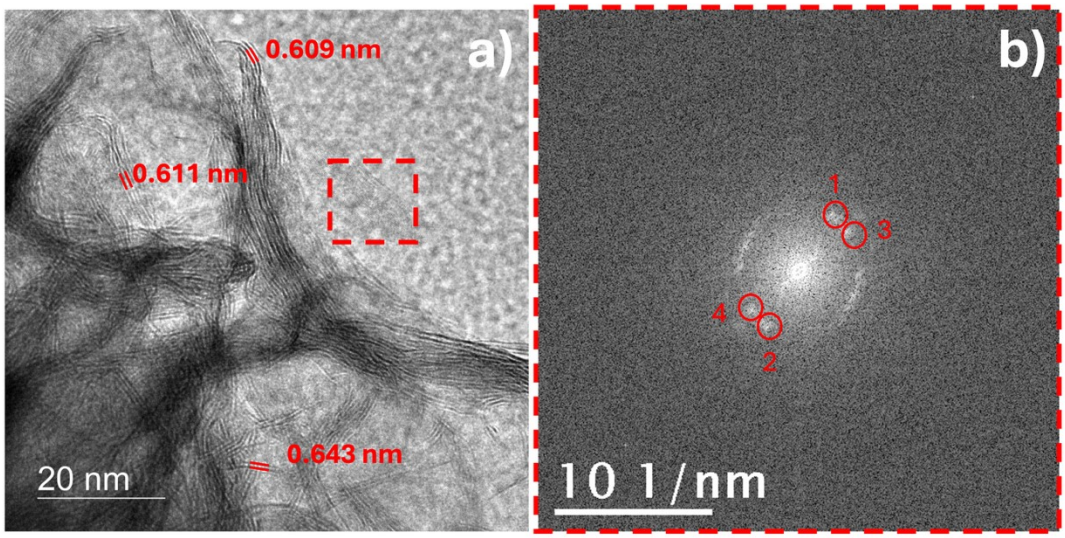

Figure S5. a) High-resolution TEM image of HCS@MoS_2, showing lattice fringes associated with the nanosheet structure; the region selected for reciprocal-space analysis is highlighted. b) FFT pattern obtained from the highlighted area, displaying well-defined reciprocal-space spots that confirm the lattice periodicity of the MoS_2 nanosheets.

HCS pore analysis

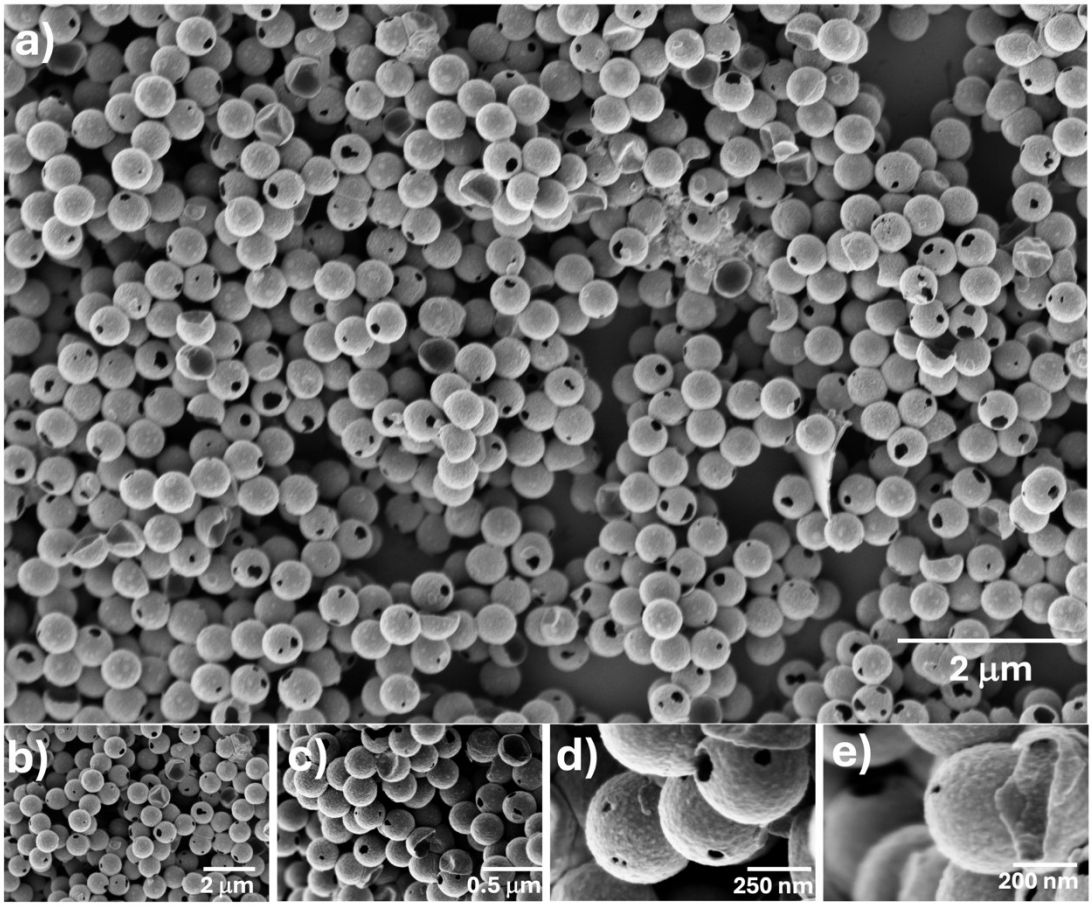

Figure S6. SEM images of HCS showing the hollow spherical morphology and the presence of surface pores across the carbon shells from low to high magnifications (a-e) with pores diameters varying from 10 to 70 nm. High-magnification panels (d–e) highlight well-defined openings that confirm the porous texture of the material.

High resolution spectra XPS for HCS@MoS_2 Samples

The high-resolution Mo 3d spectrum of HCS@MoS_2 in Fig. S7.a exhibits the characteristic doublet of Mo^{4+} corresponding to the 2H phase of MoS_2, with Mo $3d_{5/2}$ and Mo $3d_{3/2}$ peaks located at approximately 230.1 eV and 233.3 eV. In addition to these components, a second pair of features is observed at slightly lower binding energies, shifted by roughly 1 eV relative to the main Mo^{4+} doublet. Such shifts are typically associated with the metallic 1T phase of MoS_2, which presents increased electronic density at Mo sites and therefore lower binding energy. This combination of doublets indicates that the sample contains a mixture of 2H and 1T coordination environments, consistent with other results showed in the manuscript. A weak contribution at higher binding energy, around 235.3 eV, is attributed to Mo^{6+} species arising from additional oxidation and the peak located around 225 eV is attributed to S 2s contribution. The S 2p

region in Fig. S7.b shows the expected doublet for S^{2-} in MoS_2, with S $2p_{3/2}$ and S $2p_{1/2}$ appearing at approximately 163.0 and 164.1 eV, reflecting sulfur atoms coordinated to molybdenum in both 2H and 1T environments. A low-intensity signal near 168 eV is assigned to oxidized sulfur species, likely originating from slight surface oxidation or adsorbed sulfate-like groups. The overall positions and shapes of the Mo and S doublets are consistent with mixed-phase MoS_2.

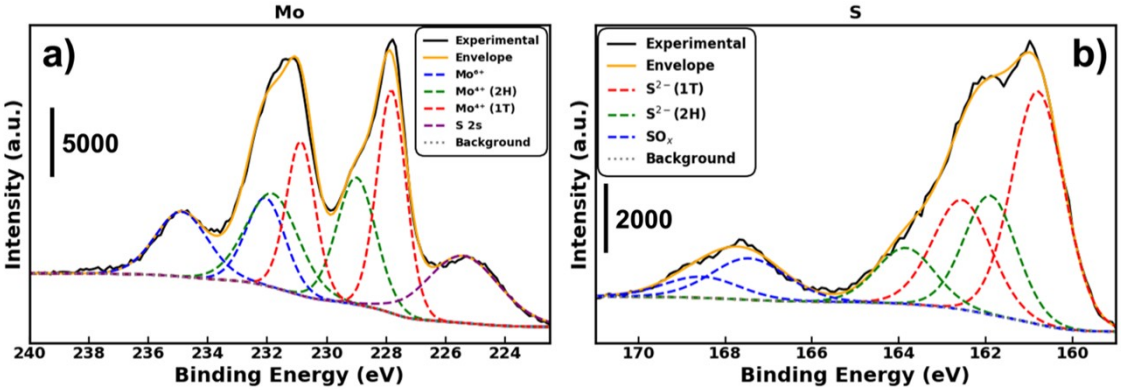

Figure S7. High resolution XPS for a) Mo and b) S.

SEM Image of HCS@MoS_2 on pyrolyzed paper

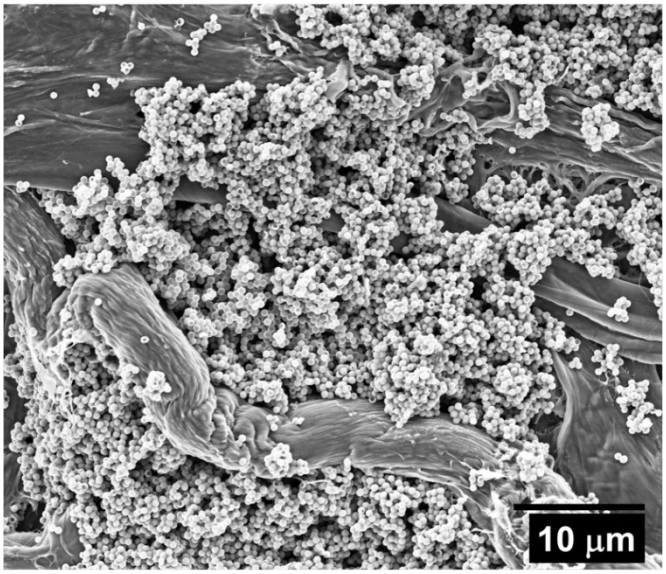

Figure S8. Arrangement of HCS@MoS2 on the fibers of the pyrolyzed paper.

Literature Comparison

Table S1. Benchmark comparison with state-of-the-art HER catalysts from the literature.

Material	η_{10}	Taffel Slope
Pt/C (commercial)[5]	~40 mV	~30 mV dec^{-1}
Pt/C (Synthesized)[6,7]	~50 mV	120, 30 mV dec^{-1}
Porousized MoS_2[8]	300 mV	84 mV dec^{-1}
1T/2H Hybrid MoS_2[9]	212 mV	78 mV dec^{-1}
MoS_2 single flake with S vacancies [10]	372 mV	135 mV dec^{-1}
sulfur-deficient MoS_2 ($MoS_{0.5}$) [11]	206 mV	113 mV dec^{-1}
HCS@MoS_2 (This work)	300 mV	167 mV dec^{-1}

Cyclic Voltammetry

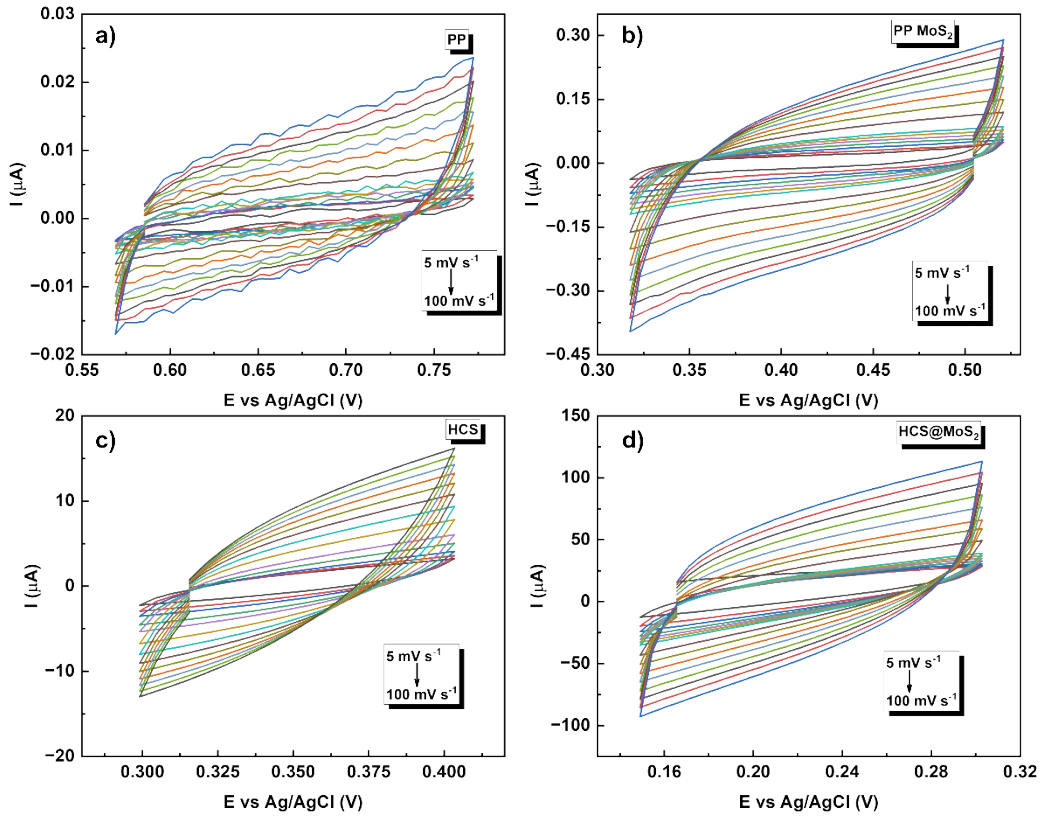

Figure S9. Cyclic voltammetry for a) PP, b) PP MoS2, c) HCS and d) HCS@MoS2 at different scanning velocity.

Morphology after stability cycles

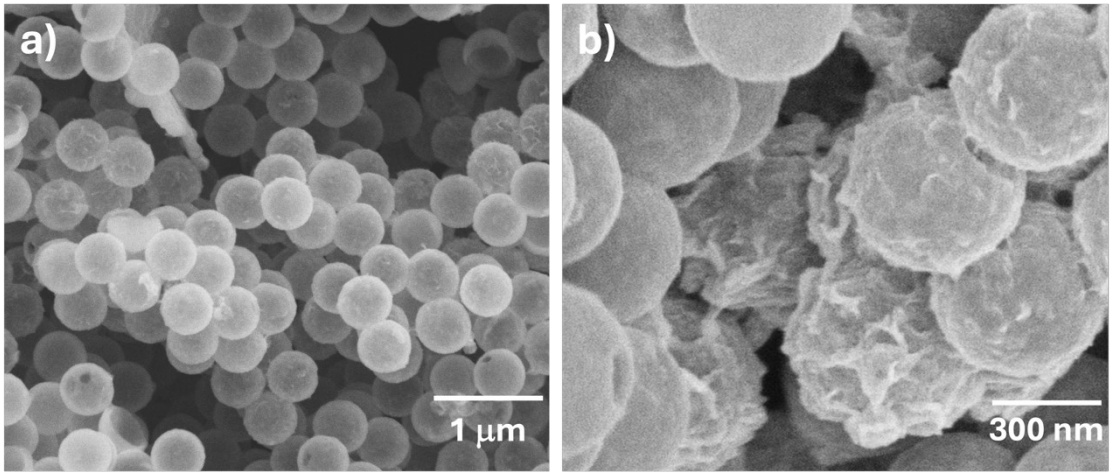

Figure S10. HCS@MoS_2 SEM images after 500 cycles with a) lower and b) higher magnification.

Phase structure after stability cycles

Figure S11 presents the high-resolution Mo 3d and S 2p spectra of HCS@MoS_2 after 500 electrochemical cycles. The Mo 3d region retains the characteristic Mo^{4+} doublets associated with the 2H and 1T phases, confirming that the mixed-phase remains after cycling. A noticeable increase in the Mo^{6+} contribution indicates surface oxidation induced by the electrochemical environment. Similarly, the S 2p spectra preserve the S^{2-} doublets at ~163.0 and 164.1 eV, while exhibiting additional broadening and a stronger SOx signal near 168 eV, consistent with surface sulfur oxidation.

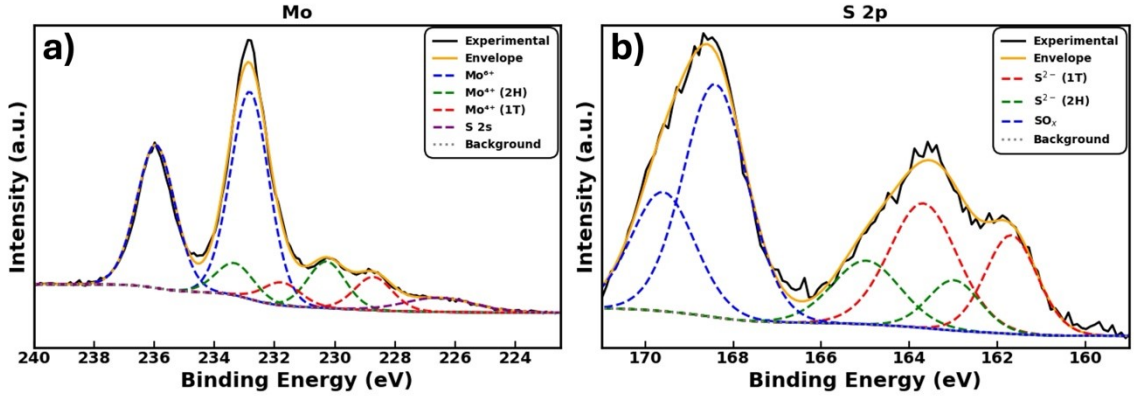

Figure S11. High resolution XPS for a) Mo and b) S after 500 cycles.

References

1 J. F. Rocha, J. C. De Oliveira, J. Bettini, M. Strauss, G. S. Selmi, A. K. Okazaki, R. F. De Oliveira, R. S. Lima and M. Santhiago, *ACS Meas. Sci. Au*, 2024, **4**, 188–200.

2 L. H. Hasimoto, J. Bettini, E. R. Leite, R. S. Lima, J. B. Souza Junior, L. Liu and M. Santhiago, *ACS Appl. Eng. Mater.*, 2023, **1**, 708–719.

3 R. Raja, P. Sudhagar, A. Devadoss, C. Terashima, L. K. Shrestha, K. Nakata, R. Jayavel, K. Ariga and A. Fujishima, *Chem. Commun.*, 2015, **51**, 522–525.
4 C. P. Veeramalai, F. Li, Y. Liu, Z. Xu, T. Guo and T. W. Kim, *Applied Surface Science*, 2016, **389**, 1017–1022.
5 F. Guo, T. J. Macdonald, A. J. Sobrido, L. Liu, J. Feng and G. He, *Advanced Science*, 2023, **10**, 2301098.
6 B. Jiang, S. Liu, L. Cheng, L. Zhou, H. Cui, M. Liu, M. Wen, C. Wang, W. Wang, S. Li and X. Sun, *International Journal of Hydrogen Energy*, 2024, **58**, 268–278.
7 J. N. Hansen, H. Prats, K. K. Toudahl, N. Mørch Secher, K. Chan, J. Kibsgaard and I. Chorkendorff, *ACS Energy Lett.*, 2021, **6**, 1175–1180.
8 B. Chen, P. Hu, F. Yang, X. Hua, F. F. Yang, F. Zhu, R. Sun, K. Hao, K. Wang and Z. Yin, *Small*, 2023, **19**, 2207177.
9 Z. Hong, W. Hong, B. Wang, Q. Cai, X. He and W. Liu, *Chemical Engineering Journal*, 2023, **460**, 141858.
10 L. H. Hasimoto, M. F. F. Das Neves, T. M. Perfecto, J. Bettini, E. R. Leite, R. B. Capaz and M. Santhiago, *ACS Appl. Energy Mater.*, 2025, acsaem.5c02263.
11 S. Saleem, M. Salman, S. Ali, Y. Ling and M. Khan, *International Journal of Hydrogen Energy*, 2022, **47**, 7713–7723.